The Twist Profile in the Cross Section of Interplanetary Magnetic Clouds

Ake Zhao[1,2] , Yuming Wang[3,4] , Hengqiang Feng[5] , Mengjiao Xu[3], Yan Zhao[5], Guoqing Zhao[5] , and Qiang Hu[6]
[1] College of Physics and Electric Information, Luoyang Normal University, Luoyang, Henan 471934, People's Republic of China; zzukeer@mail.ustc.edu.cn
[2] Henan Key Laboratory of Electromagnetic Transformation and Detection, Luoyang, Henan 471934, People's Republic of China
[3] CAS Key Laboratory of Geospace Environment, Department of Geophysics and Planetary Sciences, University of Science and Technology of China, Hefei, Anhui 230026, People's Republic of China; ymwang@ustc.edu.cn
[4] CAS Center for Excellence in Comparative Planetology, People's Republic of China
[5] Institute of Space Physics, Luoyang Normal University, Luoyang, Henan 471934, People's Republic of China
[6] Cennter for Space Plasma and Aeronomic Research, The University of Alabama in Huntsville, Huntsville, AL 35899, USA
Received 2018 September 7; revised 2018 November 25; accepted 2018 November 25; published 2018 December 10

Abstract

Magnetic flux ropes (MFRs) as a well-organized magnetic field structure embedded in space plasmas have been widely studied for several decades. The twists of magnetic field lines in MFRs can yield much information regarding the formation and stability of MFRs, yet there is still open debate about them. Here, with the aid of a uniform-twist force-free flux rope model, we study the twist profile in the cross section of a interplanetary magnetic cloud (MC) by peeling off equal azimuthal magnetic flux layer by layer from the outermost shell, just like peeling an onion. The absolute value of the average twist, $\overline{\tau}$, and the twist in each layer, τ, exhibit an almost monotonous decrease from the axis to the periphery of the MC, but τ has a larger relative error. However, they do have a coincident trend of a high-twist core and an low-twist outer shell. The twist number per unit length, $\overline{\tau}/\tau$, follows a linear trend versus $\frac{1}{\pi R}$, where R is the radius of each layer, with a correlation coefficient of 0.96/0.91 and slope of 0.27/0.26, which is well below the critical slope of 1 suggested by Wang et al.

Key words: magnetic fields – Sun: coronal mass ejections (CMEs) – Sun: heliosphere

1. Introduction

Magnetic flux rope (MFR) is one of the fundamental magnetic structures in the interplanetary medium. The flux rope structure of the interplanetary magnetic clouds (MCs) originating from the Sun have been confirmed by observational analyses and theoretical studies (Goldstein 1983; Lepping et al. 1990, 1997; Burlaga 1995; Kumar & Rust 1996). The twist distribution of the magnetic field lines inside interplanetary MCs have been a focus of study because it closely relates to the magnetic free energy and stability. Previous studies have shown that an MFR will become unstable once the total twist angle, Φ, exceeds a certain threshold, e.g., 2.5π radians for flux rope in the solar atmosphere (Hood & Priest 1981). In the latest statistical study of 115 interplanetary MCs observed by the *Wind* spacecraft (Wang et al. 2016), it was found that the twist angle of most interplanetary MFRs are larger than 2.5π radians but are well bounded by $2\frac{l}{R}$, where l is the axis length, and R is the radius of the MFR.

The local magnetic configuration of an MC could be modeled as a linear force-free flux rope with a Lundquist solution (the Lundquist model; Lundquist 1950; Lepping et al. 2006) or a nonlinear force-free flux rope with a uniform-twist solution (the GH model; Gold & Hoyle 1960). The former model suggests that the MC has a minimum finite twist at the axis and a maximum twist at the periphery, and the latter model could give the average twist of magnetic field lines in the MC. Based on magnetohydrodynamic theory, a linear force-free flux rope stays at a lower state of magnetic energy than a nonlinear force-free or non-force-free flux rope with the same helicity, hence a different profile of the twist implies a different energy state. In addition to the two fitting models above, the Grad–Shafranov (GS) reconstruction technique is an effective approach to infer the twist of MCs. Based on the assumption of a translation symmetry along the flux rope axis, i.e.,

$\partial/\partial z \approx 0$, the magnetic field components $B_x = \frac{\partial A}{\partial y}$, $B_y = -\frac{\partial A}{\partial x}$ in the transverse plane (x, y) that is perpendicular to the z-axis are obtained by Sturrock (1994), Hau & Sonnerup (1999), and Hu (2017)

$$\frac{\partial^2 A}{\partial x^2} + \frac{\partial^2 A}{\partial y^2} = -\mu_0 \frac{dP_t}{dA} = -\mu_0 j_z(A) \qquad (1)$$

in which the equi-value contours of magnetic flux function A represent transverse magnetic field lines.

Utilizing different techniques and events, researchers obtain different conclusions. For the well-known MC recorded by the *Wind* spacecraft on 1995 October 18, Larson et al. (1997) showed that the Lundquist solution matches well the field line lengths derived from velocity dispersion of energetic electrons. However, Hu & Sonnerup (2002) found that the inner magnetic field lines are more twisted than the outer ones by using the GS reconstruction. Hu et al. (2014) made a statistical study of 18 interplanetary MFRs with the aid of GS reconstruction and found that nearly one half of these events have an almost uniform twist distribution, and majority of the other flux ropes exhibit high twist at the axis, which decreases toward the edge. By using different models and methods, Hu et al. (2015) pointed out that in situ flux rope structures as derived from the GS reconstruction are more consistent with the GH model than the Lundquist model.

Recently, with the aid of a velocity-modified GH model, Wang et al. (2018) found that the twist increases together with the presence of the erosion and pancaking effects during the propagation of the MC from Mercury through Venus and Earth. Their detailed analysis suggested that the MFR probably had a high-twist core and a low-twist outer shell. Despite a number of studies on the profile of the twist in interplanetary MCs, a firm conclusion has yet to be reached. In this Letter we develop a new method using a velocity-modified GH model to
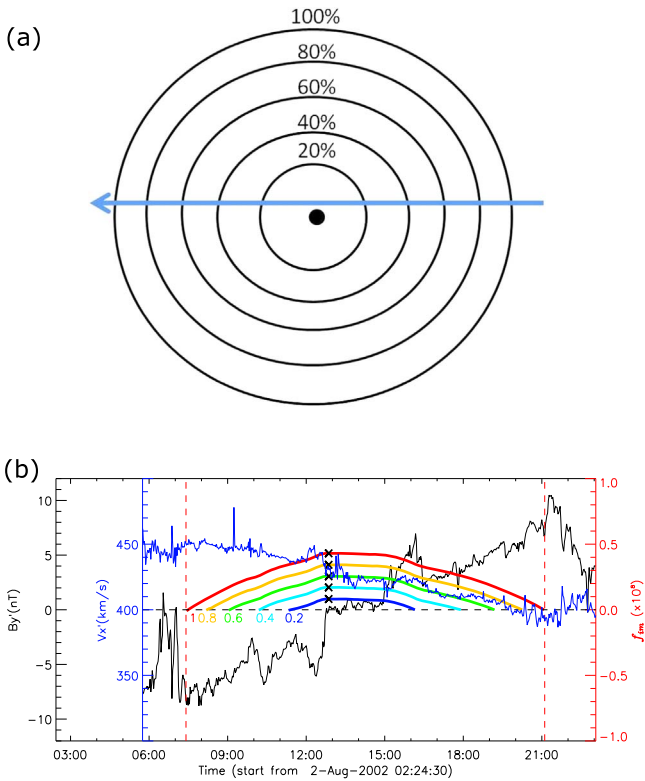
Figure 1. (a) Schematic diagram showing different fractions of azimuthal magnetic flux in the cross section of the MC; the blue arrow indicates the path of the spacecraft. (b) The vertical red dashed lines mark the boundary of the MC. Black and blue curves show the profiles of the y' component of the magnetic field and the x' component of the velocity for the entire MC in the MC frame, respectively. The five color curves show the profile of azimuthal magnetic flux (Equation (2)) for different fractions; the corresponding fraction is labeled and the black cross symbol marks the peak azimuthal magnetic flux of the corresponding fraction.

infer the twist profile in the cross section of an MC based on single-point in situ measurements of magnetic field and velocity. The GS reconstruction technique can also infer the twist distribution of the MC observed by a single spacecraft; our method is different to this, so it could act as a useful complement.

In Section 2, we describe the method and the selected event. In Section 3, the twist distribution obtained by our method is presented. We give a conclusion about the result in Section 4.

2. Method and Selection of the Event

In this Letter we use the velocity-modified GH model (Wang et al. 2016) to obtain the twist of the magnetic field line in the MC. Though the GH model describes a uniform-twist magnetic configuration, it does not mean that this model can only be used to fit the uniform-twist MFR. The model could be applied to any MFRs to provide a kind of averaged twist. Thus, in order to anatomize the twist profile in the cross section of a MFR by using the velocity-modified GH model, we peel off equal amounts of azimuthal magnetic flux, i.e., poloidal flux, layer by layer from the outer shell to the axis of the MC, as depicted in Figure 1(a). After applying the velocity-modified GH model to each peeled layer of MFR, the averaged twist $\overline{\tau}$ in the cross section of the MC can be obtained and the variation of the twist in each layer can be derived even further.

Two parameters must be noted when selecting a suitable event. One is the parameter d, i.e., the closest approach of the observational path to the MFR, which indicates how closely the path of the spacecraft crossing an MC approaches the axis of the MC. As d is in units of R and R is the radius of the flux rope, we can obtain a normalized d value, i.e., d/R. A value close to zero means that the path cuts through the inner core of the MC, and therefore the spacecraft can obtain nearly complete information from the periphery to the axis of the MC. Otherwise, the innermost part will be missed. The second parameter is the imbalance of the azimuthal magnetic flux of the MC. To ensure that equal azimuthal magnetic flux around the axis of the MC can be peeled off, we need to select the event that is not undergoing an erosion process at the front or rear boundary. During the propagation of the MCs in interplanetary space, they may interact and reconnect with the ambient interplanetary magnetic field (Tian et al. 2010; Gosling 2012) and result in an imbalanced azimuthal magnetic flux (Ruffenach et al. 2012, 2015).

For a flux rope that is not in the ongoing erosion or peeling-off phase (see the schematic diagram in Figure 8 of Wang et al. 2018), the accumulated azimuthal magnetic flux in the MC frame should be zero from one boundary to the other along the spacecraft trajectory. Here, we employ the formula developed by Dasso et al. (2006, 2007) to calculate the azimuthal magnetic flux along the path of the spacecraft in the MC frame (x', y', z'), in which the z' points along the main axis of the MC, y' is perpendicular to the observational path of the spacecraft, and x' completes the right-hand coordinate system. The azimuthal magnetic flux per unit length is estimated as

$$f_{\mathrm{im}} = \frac{F_{\mathrm{im}}}{L} = \int_{t_{\mathrm{in}}}^{t_{\mathrm{out}}} B_{y'}(t) v_{x'}(t) dt \qquad (2)$$

where L is the length along the axis of the flux rope, t_{in} and t_{out} indicate the integral interval from the front to the rear boundary, and $B_{y'}$ and $v_{x'}$ is the measured magnetic field and solar wind velocity along the y' and x' directions, respectively. The imbalance degree of the azimuthal magnetic flux is defined as $\left| \dfrac{f_{\mathrm{im}}}{f_{\mathrm{peak}}} \right|$, in which f_{peak} is the extreme value of the accumulated azimuthal flux when integrating the azimuthal flux from one boundary to the other (as shown in Figure 1(b)). If the azimuthal magnetic flux curve does not cut the abscissa when the rear boundary of the MC is reached, then the erosion occurs at the rear boundary and the excess magnetic flux accumulates at the front boundary. In such a case, the integration can begin at the rear boundary (Ruffenach et al. 2015).

Based on the description above, we check all the best-fit (i.e., fitting quality $Q = 1$) events in Table 2 in Wang et al. (2016) by applying the following two criteria: (1) the parameter d is less than 0.2, and (2) the imbalance degree of the azimuthal magnetic flux of the entire MC is less than 2%. Finally, the MC that occurred at 07:24–21:06 UT on 2002 August 2 detected by *Wind* is selected, of which d is 0.06 and the imbalance degree of the azimuthal flux for the whole MC is about 0.01.

3. Observation and Fitting Results of the MC

We use 10 minutes average plasma and magnetic field data measured by *Wind*. Figure 2 shows the MC that is characterized by enhanced magnetic field strength, smooth rotation over a large angle in the direction of the magnetic field, low proton
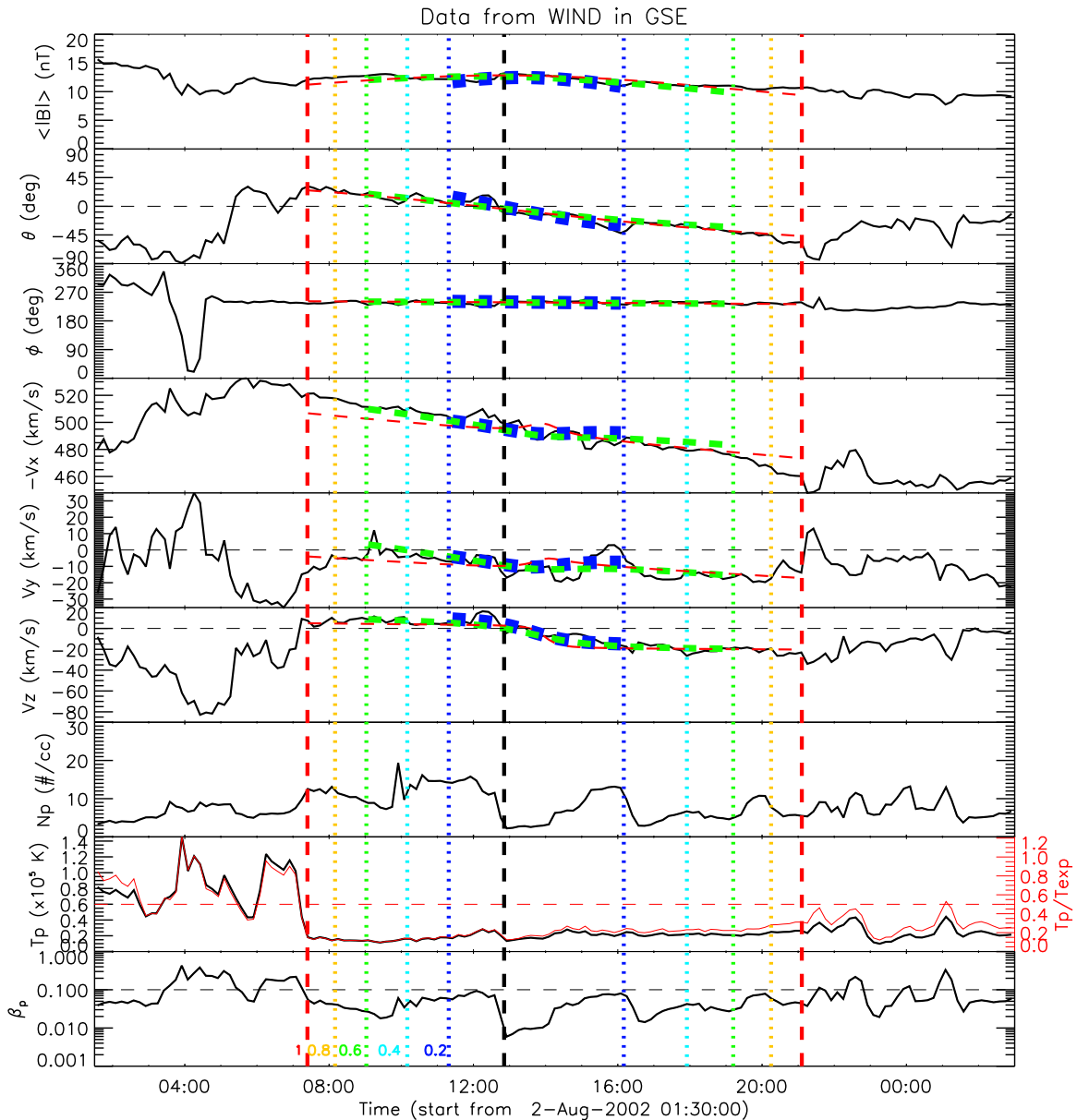
2

Figure 2. In situ observation of the MC by *Wind*. The red vertical dashed lines mark the boundary of the MC, and the vertical black dashed line denotes the time of the maximum azimuthal magnetic flux along the path of the spacecraft. From top to bottom, the panels illustrate the total magnetic field strength $\langle|B|\rangle$, the elevation angle θ and azimuthal angle ϕ of the magnetic field orientation, three components of bulk velocity in the GSE coordinate system, proton density N_p, proton temperature T_p, and proton β_p. The four vertical color dotted lines around the vertical black dashed line indicate the front and rear boundary for the 0.2, 0.4, 0.6, 0.8 fraction of the MC, and the corresponding boundary is labeled. The red, green, and blue dashed lines in the first six panels are the fitting curves of the velocity-modified GH model.

temperature, and low proton β, in which there has an evident expansion signature. This MC could be well fitted by our velocity-modified GH model; the fitting results are shown by the red dashed lines in the first six panels in Figure 2. The fitting parameters of the GH model include the elevation angle and azimuthal angle of the axis of the MC in the GSE coordinates. Using these two angles, we can convert the observed magnetic field and velocity from the GSE coordinates into the MC frame (x', y', z'), in which the MC's axis points to z'-axis and the path of the spacecraft along the x'-axis and y'-axis completes the right-hand coordinates. In the MC frame we peel off equal amounts of azimuthal magnetic flux from both the front and rear boundary of the MC, i.e., 10%–90% with a step of 10% of the peak azimuthal magnetic flux, to obtain the 90%–10% fraction of the MC. These peeled MC

fractions are further fitted by the velocity-modified GH model. The orientation of the MC axis provides key information about the consistency among the fitting results of these parts. The differences between the 10 axis orientations and the average of the 10 orientations (listed in Table 1) are all less than 15°, suggesting that the fitting results of these fractions are reliable.

Here, after peeling off equal azimuthal magnetic flux layer by layer from the periphery to the axis of the MC, and applying the velocity-modified GH model, we find the fitting results for all fractions are in good accordance with the observed data. In Figure 2, the blue, green, and red dashed lines in the first six panels show the fitting curves for 20%, 60%, and 100% fractions of the MC, respectively. The profile of azimuthal magnetic fluxes of 20%, 40%, 60%, 80%, and 100% fractions in their own frames are shown by five color curves in Figure 1(b).
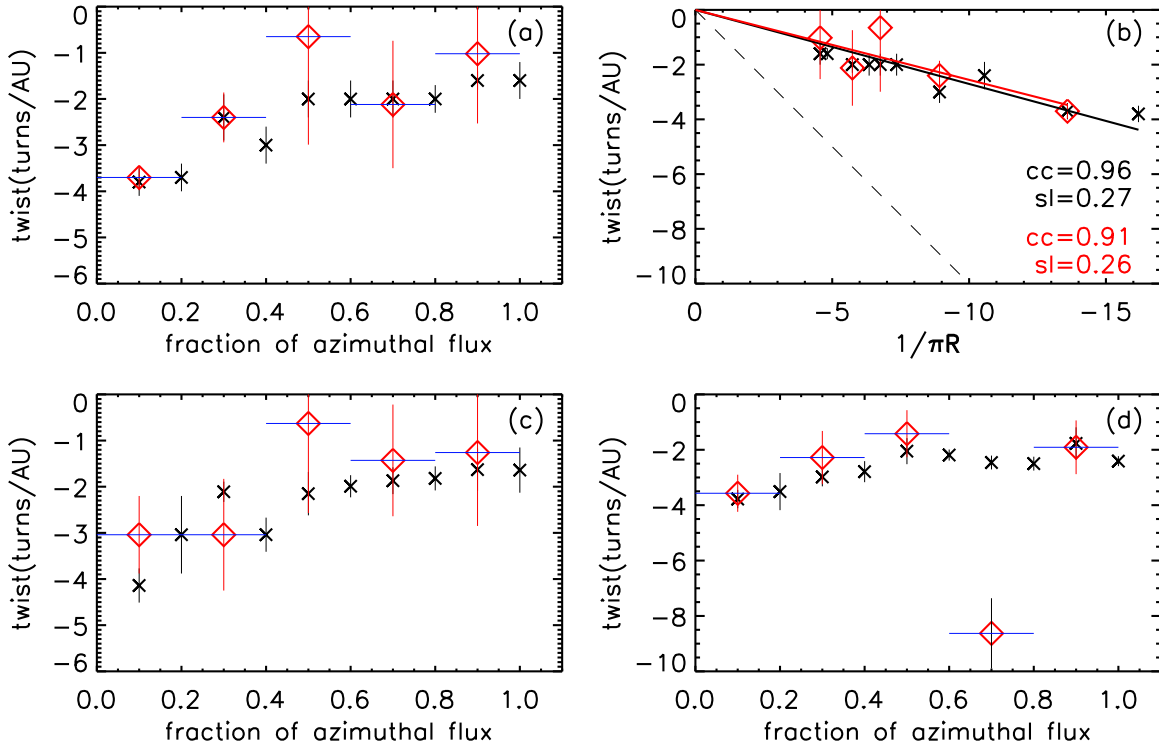
Figure 3. Twist vs. remaining fraction of azimuthal magnetic flux (a), (c), (d), and $\frac{1}{\pi R}$ (b), in which the black and red lines are linear fits. cc and sl are the correlation coefficient and the slope of linear fitting, respectively. The black symbols denote the average twist for each fraction, and the red symbols denote the twist for each layer, i.e., 0%–20%, 20%–40%, 40%–60%, 60%–80%, 80%–100%, in all panels. The blue lines indicate the layer for the corresponding azimuthal magnetic flux. All of the data in panel (a) and (b) come from Table 1. The test results come from the effect of adding 5% average normalized noise in panel (c) and changing the orientation of the MC axis in panel (d) to the mean value of the 10 orientations (see Table 1).

Table 1
Parameters for Different Fractions of Azimuthal Magnetic Flux Obtained by the Velocity-modified GH Model and GS Reconstruction

Fraction	AxialD	$\overline{\tau}$ (turns/au)	B_0 (nT)	Radius (au)	Azimuthal Flux (10^{20} Mx)	τ (turns/au)
10%	6°	$-3.8^{+0.3}_{-0.3}$	13.11	0.020	3.1 ± 0.9	$-3.7^{+0.3}_{-0.3}$
20%	2°	$-3.7^{+0.3}_{-0.3}$	12.79	0.023	4.1 ± 1.1	
30%	2°	$-2.4^{+0.5}_{-0.5}$	12.61	0.030	4.5 ± 1.7	$-2.4^{+0.5}_{-0.5}$
40%	10°	$-3.0^{+0.4}_{-0.4}$	13.29	0.035	7.4 ± 2.3	
50%	1°	$-2.0^{+0.4}_{-0.4}$	12.47	0.043	7.2 ± 2.9	$-0.7^{+2.3}_{-2.3}$
60%	1°	$-2.0^{+0.4}_{-0.4}$	12.65	0.047	8.6 ± 2.9	
70%	3°	$-2.0^{+0.4}_{-0.4}$	12.79	0.050	9.9 ± 3.0	$-2.1^{+1.4}_{-1.4}$
80%	1°	$-2.0^{+0.3}_{-0.3}$	12.82	0.055	11.7 ± 3.7	
90%	13°	$-1.6^{+0.2}_{-0.2}$	12.67	0.066	13.3 ± 5.1	$-1.0^{+1.5}_{-1.5}$
100%	13°	$-1.6^{+0.4}_{-0.4}$	12.75	0.070	14.9 ± 5.5	...
100%(GS)	12°	-1.6	...	...	14.72	...

Note. MC interval of GH model: 2002 August 2 07:24 UT–2002 August 2 21:06 UT; MC interval of GS reconstruction: 2002 August 2 07:21 UT–2002 August 2 21:03 UT; column 1 is the remain fraction of the peak azimuthal magnetic flux of the whole MC. The average values of twist, magnetic field, radius, and azimuthal magnetic flux for each fraction are listed in columns 3, 4, 5, and 6, respectively. Column 2 shows the differences between the axis orientation for each fraction of the MC and the average of 10 orientations. The last column is the twist values from the Equation (5). The two bottom rows compare the full MC analyzed by the GH model and GS reconstruction.

After peeling off the azimuthal magnetic flux as in Figure 1(a), the average twist $\overline{\tau}$ for each fraction of the MC can be obtained; this is listed in Table 1, where the positive/negative value of $\overline{\tau}$ means the handedness of the MFR is right/left-handed. To further obtain the twist distribution in the MC, we need to calculate the twist τ in each layer. By assuming that the field components B_φ and B_z are approximately uniform in each layer, we have the poloidal flux in each layer per unit length

$$\Delta\Phi_p = \int_{r_{i-1}}^{r_i} B_\varphi dr = B_{\varphi i}(r_i - r_{i-1}) \tag{3}$$

and the axis flux in each layer

$$\Delta\Phi_z = \int_0^{2\pi} d\theta \int_{r_{i-1}}^{r_i} rB_z dr = \pi B_{zi}(r_i^2 - r_{i-1}^2) \tag{4}$$
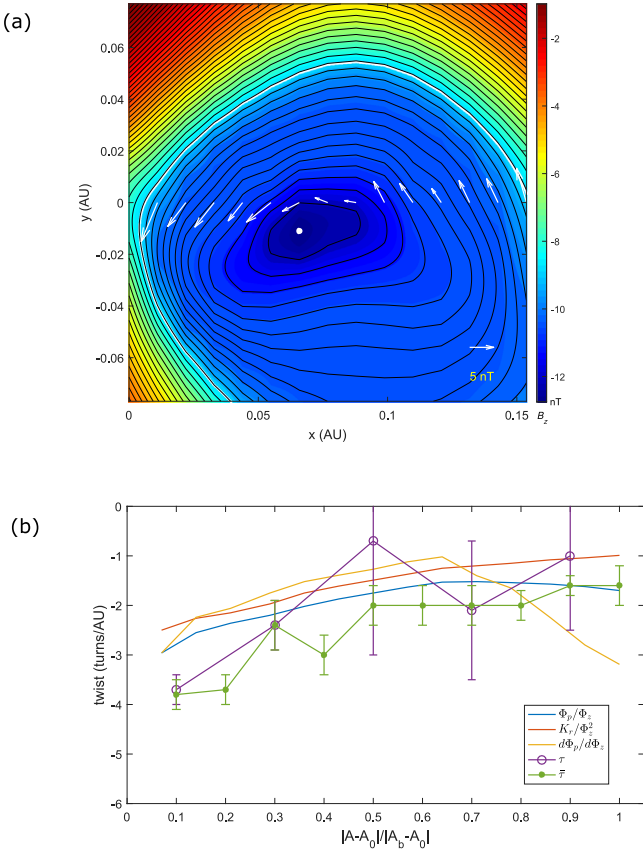
(a)

(b)

Figure 4. (a) Reconstructed cross-section map traversed by *Wind* and the axial field $B_z(A)$ filled contours in color. The white contour line indicates the boundary $A = A_b$ and the white arrows mark the measured transverse magnetic field along the path of the spacecraft ($y = 0$). The maximum axial magnetic field is marked by a white dot and $A = A_0$. (b) Change of the twist with $|A - A_0|/|A_b - A_0|$ (see the text for more details).

then

$$\frac{\Delta\Phi_p}{\Delta\Phi_z} = \frac{\Phi_{pi} - \Phi_{pi-1}}{\Phi_{zi} - \Phi_{zi-1}} = \frac{B_{\varphi i}}{2\pi B_{zi}\frac{r_i + r_{i-1}}{2}} = \tau_i. \quad (5)$$

Because the axial and poloidal magnetic fluxes per unit length can be obtained by the Equation (10) and (11) in Wang et al. (2016)

$$\Phi_z = \frac{B_0}{4\pi\overline{\tau}^2}\ln(1 + 4\pi^2\overline{\tau}^2 R^2) \quad (6)$$

$$\Phi_p = \frac{B_0}{4\pi\overline{\tau}}\ln(1 + 4\pi^2\overline{\tau}^2 R^2) \quad (7)$$

where B_0 is the magnetic field, and R is the radius of the MFR. Consequently, the number of turns per unit length in each layer can be obtained. The twist in each layer for 0%–20%, 20%–40%, 40%–60%, 60%–80%, 80%–100% are listed in the last column in Table 1, in which the uncertainty in τ_i is propagated from the uncertainty of the $\overline{\tau}_i$.

Figure 3(a) shows the average twist and the twist in each layer distribution with the fraction of azimuthal magnetic flux, where the absolute value of both kinds of twist have a roughly monotonous trend of decreasing from near the axis to the boundary of the MC, meaning that there is a maximum twist near the axis of the MC and a minimum twist near the boundary

of the MC. Wang et al. (2016) suggested that the critical total twist angle, Φ_c, is a function of the aspect ratio (the ratio of the axial length l to the radius R) of an MFR, i.e.,

$$\Phi_c = 2\frac{l}{R}. \quad (8)$$

According to this relation, the critical number of turns per unit length of the field lines winding around the axis should be

$$\tau_c = \frac{\Phi_c}{2\pi l} = \frac{1}{\pi R}. \quad (9)$$

To compare our results with Equation (9), we linearly fit the $(\tau, \frac{1}{\pi R})$ data points in Figure 3(b). The linear correlation coefficient of the $\overline{\tau}/\tau$ is about 0.96/0.91 and the slope is about 0.27/0.26 less than the critical slope of 1.

Considering that errors are an important means for deriving the twist distribution in the MC, in order to further check the reliability of our results we perform two tests: (1) for the effect of noise on the fitting results, we add 5% average randomized noise into the original measurements, and (2) for the effect of the orientation of the MC axis on the fitting results, we change the orientation to the average of the 10 orientations (listed in Table 1) when we fit the data. After repeating the above analytical process, the twist profiles (in Figures 3(c) and (d)) exhibit similar trends as those in Figure 3(a).

As mentioned in the Introduction, GS reconstruction is also a method used to infer the twist distribution of the MC, where the physical quantities, e.g., the axial (poloidal) magnetic flux, Φ_z (Φ_p), and the relative magnetic helicity, κ_r, can be calculated. According to the field twist estimation, Φ_p/Φ_z, κ_r/Φ_z^2, and $d\Phi_p/d\Phi_z$ can be utilized to infer the twist distribution of the MC. Φ_p/Φ_z and κ_r/Φ_z^2 estimate the average twist across the rope, while $d\Phi_p/d\Phi_z$ measures the twist in each layer. Figure 4(b) shows the twist distribution versus the function of $|A - A_0|/|A_b - A_0|$, in which the green line shows the change of average twist value $\overline{\tau}$ with different fractions and the purple line shows the twist distribution in each layer (data from Table 1). The trends of the Φ_p/Φ_z and κ_r/Φ_z^2 curves agree with our result $\overline{\tau}$, except that the absolute value of the twist achieved using our method is slightly larger than that achieved using the GS technique, which has been discussed in Wang et al. (2016). Though the average twist obtained by different methods does have some minor differences, the trends are basically consistent. The trend of τ appears to be decreasing more quickly than $d\Phi_p/d\Phi_z$ before 50% fraction of the MC, but increasing more slowly than it toward the boundary. Owing to the large relative error for τ, it is difficult to make an accurate comparison with the GS result. Regarding $d\Phi_p/d\Phi_z$, an effect occurs near the boundary when the contour loops are no longer closed in the direction of the boundary. Therefore, toward the boundary $d\Phi_p$ is estimated accurately, but $d\Phi_z$ is underestimated as discussed by Hu et al. (2014, their Appendix). Consequently, this effect leads to an enlarged ratio, which then overestimates the twist. Some parameters from the GS reconstruction, such as event interval, twist value, z-axis orientation difference between the GH model and GS reconstructions, and flux contents, are listed in Table 1. These results are in accordance with the GH model, hence, the twist distribution from the GS reconstruction supports the validity of our method.

4. Conclusion

In this Letter, we investigate the twist distribution in the cross section of an interplanetary MC detected by *Wind*. With the aid of the velocity-modified GH model, Wang et al. (2018) obtained the twist distribution of an MC at different heliocentric distances. Here, we developed a new method to infer the twist distribution for a particular MC traversed by a single spacecraft using the same model. By peeling off equal azimuthal magnetic flux from both the front and rear boundary, just like peeling an onion, the average twist and the twist in each layer of the cross section of the MC can be inferred. We find that the absolute value of twists exhibit a roughly monotonous decrease from the axis to the edge. The result is generally in agreement with the GS reconstruction, and means that the MC has a higher-twist core and a lower-twist outer shell, which is consistent with the recent study by Wang et al. (2018).

ORCID iDs

Ake Zhao ⓞ https://orcid.org/0000-0002-6740-2659
Yuming Wang ⓞ https://orcid.org/0000-0002-8887-3919
Hengqiang Feng ⓞ https://orcid.org/0000-0003-2632-8066
Guoqing Zhao ⓞ https://orcid.org/0000-0002-1831-1451
Qiang Hu ⓞ https://orcid.org/0000-0002-7570-2301

References

Burlaga, L. F. 1995, Interplanetary Magnetohydrodynamics (Oxford: Oxford Univ. Press)
Dasso, S., Mandrini, C. H., Démoulin, P., & Luoni, M. L. 2006, A&A, 455, 349
Dasso, S., Nakwacki, M. S., Démoulin, P., & Mandrini, C. H. 2007, SoPh, 244, 115
Gold, T., & Hoyle, F. 1960, MNRAS, 120, 89
Goldstein, H. 1983, in JPL Solar Wind Five, ed. M. Neugebauer (Washington, DC: NASA), 731
Gosling, J. T. 2012, SSRv, 172, 187
Hau, L.-N., & Sonnerup, B. U. Ö. 1999, JGR, 104, 6899
Hood, A. W., & Priest, E. R. 1981, GApFD, 17, 297
Hu, Q. 2017, ScChE, 60, 1466
Hu, Q., Qiu, J., Dasgupta, B., Khare, A., & Webb, G. M. 2014, ApJ, 793, 53
Hu, Q., Qiu, J., & Krucker, S. 2015, JGRA, 120, 5266
Hu, Q., & Sonnerup, B. U. Ö. 2002, JGR, 107, 1142
Kumar, A., & Rust, D. M. 1996, JGR, 101, 15667
Larson, D. E., Lin, R. P., McTiernan, J. M., et al. 1997, GeoRL, 24, 1911
Lepping, R. P., Berdichevsky, D. B., Wu, C.-C., et al. 2006, AnGeo, 24, 215
Lepping, R. P., Burlaga, L. F., Szabo, A., et al. 1997, JGR, 102, 14049
Lepping, R. P., Jones, J. A., & Burlaga, L. F. 1990, JGR, 95, 11957
Lundquist, S. 1950, Ark. Fys., 2, 361
Ruffenach, A., Lavraud, B., Farrugia, C. J., et al. 2015, JGRA, 120, 43
Ruffenach, A., Lavraud, B., Owens, M. J., et al. 2012, JGRA, 117, A09101
Sturrock, P. A. 1994, Plasma Physics, An Introduction to the Theory of Astrophysical, Geophysical and Laboratory Plasmas (Cambridge: Cambridge Univ. Press)
Tian, H., Yao, S., Zong, Q., He, J., & Qi, Y. 2010, ApJ, 720, 454
Wang, Y., Shen, C., Liu, R., et al. 2018, JGRA, 123, 3238
Wang, Y., Zhuang, B., Hu, Q., et al. 2016, JGRA, 121, 9316